Impacts of traffic emissions on atmospheric particulate nitrate and organics at a downwind site on the periphery of Guangzhou, China

Yi Ming Qin[1], Hao Bo Tan[2], Yong Jie Li[3,*], Misha I. Schurman[4], Fei Li[2], Francesco Canonaco[5], André S. H. Prévôt[5], Chak K. Chan[1,4,6,*]

[1]Department of Chemical and Biomolecular Engineering, Hong Kong University of Science and Technology, Hong Kong, China
[2]Key Laboratory of Regional Numerical Weather Prediction, Institute of Tropical and Marine Meteorology, China Meteorological Administration, Guangzhou, China
[3]Department of Civil and Environmental Engineering, Faculty of Science and Technology, University of Macau, Taipa, Macau, China
[4]Division of Environment, Hong Kong University of Science and Technology, Hong Kong, China
[5] Laboratory of Atmospheric Chemistry, Paul Scherrer Institute, 5232, Villigen PSI, Switzerland
[6]School of Energy and Environment, City University of Hong Kong, Hong Kong, China

[*]To whom correspondence should be addressed

Chak K. Chan: AC1-G5716, School of Energy and Environment, City University of Hong Kong, Tat Chee Avenue, Kowloon, Hong Kong, China
Tel: (852) 3442-5593; Fax: (852) 3442-0688
Email: chak.k.chan@cityu.edu.hk

Yong Jie Li: E11-3017, Faculty of Science and Technology, University of Macau, E11, Avenida da Universidade, Taipa, Macau, China
Tel: (853) 8822-4943; Fax: (853) 8822-2426
Email: yongjieli@umac.mo

Abstract:

Particulate matter (PM) pollution on the peripheries of Chinese megacities can be as serious as in cities themselves. Given the substantial vehicular emissions in inner-city areas, the direct transport of primary PM (e.g. black carbon and primary organics) and effective formation of secondary PM from precursors (e.g. NO_x and volatile organic compounds) can contribute to PM pollution in "buffer" zones between cities. To investigate how traffic emissions in inner-city areas impact these adjacent "buffer" zones, a suite of real-time instruments were deployed in Panyu, downwind from central Guangzhou, from November to December 2014. Nitrate mass fraction was higher on high-PM days, with the average nitrate-to-sulfate ratio increasing from around 0.35 to 1.5 as the PM mass concentration increased from 10 to 160 $\mu g/m^3$. Particulate nitrate was strongly correlated with excess ammonium ($[NH_4^+]/[SO_4^{2-}]$ - 1.5) × $[SO_4^{2-}]$), with higher concentrations in December than in November due to lower temperatures. The organic mass fraction was the highest across all PM_1 levels throughout the campaign. While organic aerosols (OA) were dominated by secondary organic aerosols (SOA = semi-volatile oxygenated organic aerosols + low-volatility oxygenated organic aerosols) as a campaign average, freshly-emitted hydrocarbon-like organic aerosols (HOA) contributed up to 40% of OA during high-OA periods that typically occurred at nighttime and contributed 23.8% to 28.4% on average. This was due to daytime traffic restrictions on heavy-duty vehicles in Guangzhou, and HOA almost increased linearly with total OA concentration. SOA increased as odd oxygen (O_x = O_3 + NO_2) increased during the day due to photochemistry. A combination of nighttime traffic emissions and daytime photochemistry contributed to the buildup of PM in Panyu. The mitigation of PM pollution in inner-city areas by reducing vehicular traffic can potentially improve air quality in peripheral areas.

1. Introduction:

Traffic emissions are one of the main contributors to air quality deterioration in rapidly expanding urban China (Kelly and Zhu, 2016; Zhang et al., 2017). Pollutants emitted from vehicles, such as NO_x, volatile organic compounds (VOCs), black carbon (BC) and other traffic-related particulate matter (PM), have increased over last decades (Wang et al., 2013; Zhang et al., 2012). Apart from the primary PM, the oxidation of traffic-related gaseous pollutants such as NO_x, VOCs, semi-volatile VOCs (SVOCs) and low-volatility VOCs (LVOCs) leads to the formation of particulate nitrate and secondary organic aerosols (SOA), exacerbating PM pollution. Multiple studies have

32 shown that the concentrations and proportions of nitrate in PM have increased significantly in most

33 Chinese megacities (Pan et al., 2016; Wen et al., 2015; Xue et al., 2014).

34 The rapid economic development in the Pearl River Delta (PRD) region has led to a rapid

35 deterioration in air quality, especially due to a sharp increase in PM (Chan and Yao, 2008; Ho et

36 al., 2003; Li et al., 2017). With densely populated cities including two megacities, Guangzhou and

37 Shenzhen, and other smaller cities, the PRD region is developing into a giant city cluster. There

38 are, nevertheless, less populated areas between these cities that can serve as a "buffer" zone in

39 terms of regional air quality. Due to air dispersion patterns and regulatory strategies, air pollutants

40 in highly urbanized regions can greatly influence PM levels in peripheral regions. For example,

41 highly-polluting vehicles such as heavy-duty diesel trucks are banned from the inner areas of many

42 Chinese megacities during the day but are nevertheless active at night and in the early morning,

43 especially on the peripheries of these megacities. This regulatory policy has resulted in nighttime

44 peaks in vehicular pollutants, which have been commonly observed in many Chinese cities (Zhang

45 and Cao, 2015). Although vehicle emissions are substantially reduced relative to the without

46 control scenarios, there was still significantly higher emission density in East China than in

47 developed countries with longer histories of vehicle emission control (Wu et al., 2016). Given the

48 complex and non-linear processes involved in the secondary production of PM such as nitrate and

49 organic aerosols, the impacts of these adjacent "buffer" zones on air quality are crucial. However,

50 relatively little attention has been paid to how air pollutants in major cities affect these adjacent

51 areas.

52 Panyu District lies directly south of central Guangzhou and experiences predominantly

53 northerly/northeasterly winds between September and February (Zou et al., 2015). A campaign

54 with a host of real-time instruments including an Aerodyne HR-ToF-AMS was conducted at a site

55 in Panyu from November to December 2014 and provides a unique opportunity to explore how

56 pollutants from the city center have impacted this adjacent "buffer" zone, especially in terms of

57 nitrate and secondary organic aerosols. As will be shown, the mass fraction of nitrate increased as

58 PM_1 increased, and the organic mass fraction was the highest among PM_1 species across all PM_1

59 levels. A comprehensive analysis of nitrate and organics and their interplay with meteorological

60 parameters will be presented. Primary OA (e.g. HOA) and SOA from traffic-related VOC

61 precursors will also be discussed. Our findings can provide useful information for regional

62 emission control strategies covering urban and "buffer" areas and improving parameterization in
63 air quality models.

2. Method

2.1. Sampling site description
66 Guangzhou Panyu Atmospheric Composition Station (GPACS), a China Meteorological
67 Administration site, is located at the summit of Dazhengang ($23°00$ N, $113°21$ E) at an altitude of
68 approximately 150 m (Fig. S1 in the Supplement). The site is approximately 15 km south of the
69 city center and surrounded by residential neighborhoods with no significant industrial sources
70 nearby (Tan et al., 2013; Cheung et al., 2016). Ambient sampling was conducted from November
71 7th, 2014 to January 3rd, 2015.

2.2. Measurements
74 In the HR-ToF-AMS measurements (DeCarlo et al., 2006), ambient air was sampled through a
75 $PM_{2.5}$ cyclone on the rooftop with a flow rate of approximately 0.084 L/min drawn by the AMS
76 and the remainder drawn by an auxiliary pump. A diffusion drier was used to dry the sampled air
77 stream, which reduced the RH of the air to below 30% before entering the HR-ToF-AMS. Other
78 data presented in this work were obtained from collocated instruments including a Grimm 180 for
79 $PM_{2.5}$, a thermo-optical ECOC analyzer (Sunset Laboratory Inc.), a Magee AE33, a dual spot filter-
80 based instrument for black carbon (Drinovec et al., 2015), a gas analyzer system (Teledyne
81 Instruments), and a monitor for aerosols and gases in ambient air (MARGA, Metrohm applikon)
82 with a $PM_{2.5}$ cutoff. The $PM_{2.5}$ mass concentration as measured with a Grimm 180 was corrected
83 using the daily $PM_{2.5}$ mass concentration through quartz filter measurement (Text S1).
84 Meteorological data (e.g. wind, temperature and RH) were obtained from a weather station located
85 near the sampling site. Solar irradiance data were measured from a station in Nansha District,
86 around 27.5 km from the sampling site. Particle liquid water content (LWC) was estimated with
87 an aerosol inorganic model (E-AIM II) (Clegg et al., 1998).

88 The AMS collected five-minute average particle mass spectra spanning from m/z 12 to 300 for
89 the V+ particle time-of-flight (pToF) mode (high sensitivity) and the W mode (high resolution).
90 The high-resolution only analyzed the signals with m/z below 200. AMS calibrations, including
91 ionization efficiency (IE) calibration, flow rate calibration, and size calibration, were used as well

92   as data quality assurance protocols (DeCarlo et al., 2006; Lee et al., 2013; Schurman et al., 2015).

93   IE calibrations with DMA size-selected (mobility diameter, D_m= 400 nm) pure ammonium nitrate

94   particles were carried out weekly. Ambient air filtered with a HEPA filter was sampled on a daily

95   basis for 30 minutes to obtain background signals. Flow rate was made with a Gilian Gilibrator.

96   PToF size calibrations were made with Nanosphere TM PSL particles (Duke Scientific, Palo Alto,

97   CA, USA) and ammonium nitrate particles in the size range of 178 to 800 nm (selected with a

98   scanning mobility particle sizer). Both flow rate and size calibration were performed before and

99   after the sampling campaign. Gaseous CO_2 concentrations were measured with a CO_2 monitor

100 (PICARRO 2301) to quantify their contributions to m/z 44 signal intensities.

2.3. Data analysis

103 AMS data analysis was performed using the SQUIRREL (v1.56D) and PIKA (v1.15D) toolkits

104 written in Igor Pro 6.37A (WaveMetrics Inc., Lake Oswego, OR). Default relative ionization

105 efficiency (RIE) values of 1.2 for sulfate, 1.1 for nitrate, 1.3 for chloride, and 1.4 for organics were

106 used. The ammonium RIE of 4.7 was chosen as the average from IE calibrations. A particle

107 collection efficiency factor (CE) of 0.7 was used to account for particle losses within the instrument.

108 The influence of RH in this study was minor, as a diffusion drier was used to maintain the sampling

109 line RH consistently below 30%. Under these conditions, Middlebrook's parameterization

110 suggests a CE of ~45–50% based on the measured inorganic constituents (Middlebrook et al.,

111 2012). However, organic compounds, which are less bouncy than inorganics, dominated at the

112 measurement site. They can also hinder the complete efflorescence of particles in the drier and

113 further reduce the particle bounce effect and increase particle collection efficiency. The mass

114 concentrations of PM_1 (sum of NR-PM_1 and BC) were comparable to those of $PM_{2.5}$ with a slope

115 of 1.1 and Pearson correlation coefficient (R_p) of 0.95 (Fig. S2a) when using a CE of 0.7.

116 Furthermore, total AMS organics were also correlated with organic matter (OM) concentrations

117 derived from the OC measurements (Fig. S2b) with a slope of 1.1 and R_p of 0.82. The OC-to-OM

118 conversion was calculated using organic-matter-to-organic-carbon ratio (OM:OC) data from the

119 HR-ToF-AMS elemental analysis. AMS-measured sulfate, nitrate, and ammonium were

120 comparable to those measured with MARGA with slopes of 1.0, 0.9, and 0.7 respectively. These

121 comparisons suggest that a choice of CE = 0.7 is appropriate for the OA-dominating NR-PM_1 in

122 this study.

123   Source apportionment for OA was performed using the newly developed ME-2 via the SoFi

124   interface coded in Igor Pro (Canonaco et al., 2013). The procedure allows an effective exploration

125   of the solution space, a more objective selection of the optimal solution, and an estimation of the

126   rotational uncertainties (Canonaco et al., 2013; Crippa et al., 2014; Elser et al., 2016; Fröhlich et

127   al., 2015; Paatero and Hopke, 2009). We only considered ions up to m/z 100 due to the low signal-

128   to noise ratios of larger ions. Fully unconstrained runs (PMF) were first explored. However, the

129   three-factor solution suffers from the mixing of the HOA factor with the cooking organic aerosols

130   (COA) factor (Fig. S4) as well as the SVOOA factor with the biomass burning related organic

131   aerosols (BBOA) factor. The four-factor solution splits highly oxidized low-volatile OOA

132   (LVOOA) into two sub-factors (Fig. S5). The inclusion of additional factors still cannot resolve

133   pure primary OA factors (HOA, COA and BBOA) as they may have similar time series or profiles.

134   Zhang et al. (2013) also report that the PCA-resolved HOA can be affected by cooking emissions

135   with a distinct noontime peak in Beijing in spring and summer. By introducing *a priori* information

136   of source profiles for HOA, COA and BBOA, the ME-2 provides additional control over the

137   rotational ambiguity (Canonaco et al., 2013; Paatero and Hopke, 2009). The *a* value, ranging from

138   zero to unity, stands for the percentage by which each m/z signal of the final solution spectra may

139   differ from the anchor. A value of 0 means no deviation is allowed, while a value of 1 means 100%

140   deviation is allowed.

141   The OA source apportionment was performed by constraining the source profile of HOA, COA

142   and BBOA with *a* values of 0.1, 0.2, and 0.3 for HOA, COA, and BBOA respectively. The HOA

143   source profile was extracted from the data set using a separate PMF run in selected time series

144   with peaks in organic mass concentration. The COA reference was adopted from the Mong Kok

145   campaign in Hong Kong (Lee et al., 2015) while the reference BBOA profile was adopted from

146   MILAGRO (Aiken et al., 2009). A detailed discussion can be found in the supplementary

147   information (Text S2).

148   **3.   Results and Discussion:**

149   **3.1. Overall composition**

150

151   Northerly   winds   prevailed   throughout   the   entire   campaign

152   (Text S3). Located south of central Guangzhou, the sampling site was thus severely affected by

153 pollutants transported from the city center. Overall, organics accounted for 46.3 % (or 24.5 $\mu g/m^3$)

154 of the PM_1 mass on average. Sulfate, nitrate, ammonium, BC, and chloride accounted for 23.1%,

155 11.2%, 9.1%, 8.3%, and 1.9% of the PM_1 mass respectively (Fig. 1a and Fig. 1b show the

156 variations in species mass fractions in PM_1 species as a function of total PM_1 mass loading (with

157 BC inclusive) and the probability density of PM_1 mass loading respectively. The organic mass

158 fraction was the highest among all PM_1 species across all PM_1 levels. On the contrary, the mass

159 fraction of sulfate decreased from 0.25 to 0.15 as the PM_1 concentration increased from 10 to 160

160 $\mu g/m^3$. The decrease in the sulfate mass fraction was compensated for by the increased mass

161 fraction of nitrate and, to a lesser extent, chloride. The mass ratio of nitrate to sulfate in ambient

162 aerosols can be further used to evaluate the relative importance of stationary and mobile sources

163 (Arimoto, 1996; Tan et al., 2009). In our study, the average nitrate-to-sulfate ratios were around

164 0.35 when PM_1 levels were lower than 40 $\mu g/m^3$. These ratios increased significantly as the PM

165 concentration increased, reaching 1.5 on the highest-PM_1 days (averaging 160 $\mu g/m^3$), highlighting

166 the substantial contribution of vehicle emission pollutants to PM on high-PM days.

167 ## 3.2.   Nitrate formation
168
169 The increase in the relative contribution of nitrate on highly-polluted days has also been observed

170 in AMS studies at other locations in China, such as Shenzhen (He et al., 2011), Beijing (Huang et

171 al., 2010), and Changdao (Hu et al., 2013). We used the molar concentration of total nitrate

172 $[HNO_3(g) + NO_3^-(p)]$ to examine the increase in nitrate species, where $HNO_3(g)$ was measured

173 with MARGA and $NO_3^-(p)$ was measured with HR-ToF-AMS. Organic nitrates can show

174 fragments (NO^+ and NO_2^+) similar to inorganic nitrate in HR-ToF-AMS and contribute to the

175 nitrate concentration measured with AMS. Farmer et al. (2010) have used NO^+-to-NO_2^+ ratios to

176 estimate organic nitrate concentration from HR-ToF-AMS measurements. Xu et al.(2015) used the

177 NO^+/NO_2^+ values of 5 and 10, which likely correspond to the upper and lower bounds of the ratio

178 from organic nitrates. We adopt the NO^+/NO_2^+ method (hereinafter Method 1) in this study to

179 estimate the contributions of inorganic and organic nitrates. However, the vast array of possible

180 organic nitrate parent compounds in ambient particles and the variations in the NO^+/NO_2^+ ratios

181 between instruments can lead to biases in the calculations. The organic nitrate concentration can

182 also be estimated using the organic concentration and elemental ratios (OM:OC and N:C) from

183 HR-ToF-AMS measurements (Method 2) (Schurman et al., 2015b). Using these two methods (see

184   details in Text S4), the contribution from organic nitrate ranged from around 10% to 25% of the

185   total AMS-measured nitrate. In Fig. 2, the estimated inorganic nitrate tracked well ($R_p^2 \geq 0.95$,

186   0.9<Slope <1) with the total HR-ToF-AMS nitrate concentration, closely followed the 1:1 line,

187   and mostly lay in the range of the 1:1.25 and 1:0.75 lines. Furthermore, as shown in Fig. S2,

188   concentrations of nitrate from AMS were comparable to those from MARGA, with a correlation

189   slope of 0.9 and an R_p of 0.95. The influence of organic nitrates in our calculation of total nitrate

190   is expected to be minor. Given the uncertainties associated with each estimation, we use the HR-

191   ToF-AMS nitrate concentration in the following discussions.

192   In Fig. 3, the total (particle + gas) nitrate is closely correlated with NO_x during both daytime and

193   nighttime. At the same NO_x levels, total nitrate increased as O_x increased during the day (Fig. 3a),

194   suggesting the photochemical formation of nitrate. Odd-oxygen (O_x) concentrations are closely

195   linked to the extent of photochemical oxidation in an air mass. We used O_x instead of O_3 to account

196   for the titration of O_3 by freshly emitted NO, which produces NO_2. At night (Fig. 3b), O_x

197   concentrations were relatively low when NO_x concentrations were high. The slope of total nitrate

198   against NO_x during the day is steeper than that at night. The nighttime formation of nitric acid

199   involves the consumption of NO_x and O_3 (Seinfeld and Pandis, 2006). While NO_x can be

200   replenished by primary emissions, O_3 is mainly produced during the day and consumed at night.

201   Thus high total nitrate concentrations were correlated with high NO_x and low O_3 levels at night.

202   Gas-to-particle partitioning of nitrate species to form particulate nitrate can be affected by

203   concentrations of ammonium and sulfate. An increase in ammonium or a decrease in sulfate can

204   facilitate the formation of particulate nitrate (Seinfeld and Pandis, 2006). A number of studies have

205   indicated that a molar ratio of ammonium to sulfate of 1.5 demarcates the observation of particulate

206   nitrate (Griffith et al., 2015; Huang et al., 2011a; Liu et al., 2015b; Pathak et al., 2004). Under

207   ammonium-rich (AR, $[NH_4^+]/[SO_4^{2-}] > 1.5$) conditions, additional ammonia is available to transfer

208   HNO_3 to the particle phase. In contrast, under ammonium-poor (AP, $[NH_4^+]/[SO_4^{2-}] < 1.5$)

209   conditions, all of the ammonia is used to neutralize H_2SO_4 until letovicite ($(NH_4)_3H(SO_4)_2$) is

210   formed. AR conditions prevailed throughout the entire campaign. Figure 4 shows that excess

211   ammonium, defined as ($[NH_4^+]/[SO_4^{2-}]$ - 1.5) $\times [SO_4^{2-}]$), tracked well with particulate nitrate

212   concentration with a slope of 0.93. Figure 5 shows that excess ammonium tracked better with

213   nitrate than Na^+ and Ca^{2+} did (with MARGA data). The slope of nitrate to excess ammonium was

less than 1, indicating that ammonium was sufficient to neutralize the particulate nitrate. Organic acids and other unmeasured anions may account for the extra ammonium not associated with nitrate. The molar concentration of alkali cations was around 7–10 times lower than that of nitrate and their role in stabilizing nitrate was negligible in our study.

The partitioning of nitrate between the gas and particle phases shows significant differences between November and December (Fig. 6). The average ratio of nitrate to HNO_3 (the slope of the scatter plot) was 3.2 in November and 7.8 in December. NH_3 concentration in the gas phase was not a limiting factor as the concentration of NH_3 was even higher in November than in December (Fig. 6a). Lower temperatures in December shifted the equilibrium toward the particle phase, increasing the nitrate concentration in the particle phase (Fig. 6b). Higher RH or particle liquid water content favors the formation of nitrate, but the effects were not obvious (Fig. 6c, 6d).

In summary, the NO_x emissions led to nitrate formation during both daytime and nighttime. The fraction of nitrate increased and compensated for the decrease in the fraction of sulfate as the PM_1 concentration increased. Ammonium-rich conditions prevailed and particulate nitrate tracked well with excess ammonium. Lower temperature in December favors the partitioning of nitrate toward particle phase than in November.

3.3. Organics

Organics contributed most to the PM_1 mass measured in Panyu. A growing number of studies have shown that vehicle emissions are important sources of both primary and secondary organic aerosols (Deng et al., 2017; Louie et al., 2005; Platt et al., 2014). Reactive tracer gases and the primary organic pollutants can be oxidized to form SOA in urban air outflows (Gentner et al., 2017).

3.3.1. Elemental analysis of OA

Elemental analysis of OA (ratios of H:C, O:C and OM:OC) provides useful information for assessing OA characteristics and their evolution. Ions in the high-resolution mass spectra were used to calculate the elemental ratios using the Improved-Ambient method (Canagaratna et al., 2015). Results obtained from the Aiken-Ambient (Aiken et al., 2007) protocol are also listed in Table 1 for comparison with elemental ratios reported in the literature. We further used empirical

245   constants (11% for H:C, 27% for O:C, and 9% for OM:OC) from Canagaratna et al. (2015) to

246   estimate the ratios accounting for the possible underestimation of the O:C ratio in earlier studies.

247   The average O:C, H:C, and OM:OC ratios showed little variation between the two months, with

248   average values of 0.53, 1.63, and 1.87 respectively in November, and 0.53, 1.65, and 1.87

249   respectively in December. The observed elemental ratios generally agreed with other AMS-based

250   reported values in the PRD (Table 1). The H:C ratio was similar to those at rural sites in Kaiping

251   (1.64) and Heshan (1.65) and slightly higher than that in suburban Hong Kong (1.54 and 1.55) but

252   lower than those at urban sites in Shenzhen (1.81) and Mong Kok in central Hong Kong (1.84).

253   O:C and OM:OC ratios, on the contrary, were higher than those at urban sites (Shenzhen and Mong

254   Kok) and lower than that in Kaiping but similar to those in Heshan and at suburban Hong Kong.

255   Overall, the relatively low H:C ratio and high O:C ratio suggest that OA at this site have a higher

256   degree of oxygenation than those at urban sites (e.g. Shenzhen) but a lower degree than those at

257   rural sites (e.g. Kaiping). Fig. 7 shows that the diurnal variations in H:C, O:C, OM:OC and carbon

258   oxidation state ($\overline{OS_c} \approx 2 \times O:C - H:C$) were similar in November and December. The average H:C

259   ratio ranged from 1.6 to 1.7, with a pronounced increase in the late afternoon from 16:00 to 20:00,

260   and remained at a maximum until midnight due to fresh organic sources at night. The O:C and

261   OM:OC ratios and $\overline{OS_c}$ increased during the day with afternoon peaks at around 15:00, likely due

262   to high photochemical activity and the production of SOA during daylight hours.

263   **3.3.2. Sources and formation of OA**

264   The mass spectra of all OA factors and their mass concentrations obtained through PMF analysis

265   with ME-2, together with the time series of external tracers, are shown in Fig. 8. HOA correlated

266   well with NO_x since both are traffic-related species. While the mass spectrum of COA shares

267   spectral similarities with HOA, it is distinguished from that of HOA by a higher contribution of

268   $C_3H_3O^+$ at m/z 55 and a much lower contribution of ions at m/z 57 (He et al., 2010; Mohr et al.,

269   2012). The time series of COA tracked well with one of its tracer ions, $C_6H_{10}O^+$. The other primary

270   factor, BBOA, is characterized by the presence of signals at m/z 60 ($C_2H_4O_2^+$) and m/z 73

271   ($C_3H_5O_2^+$), which are typically associated with levoglucosan (Alfarra et al., 2007; Schneider et al.,

272   2006). The time series of COA and BBOA also tracked well with those of its marker ions. The two

273   oxygenated organic aerosol factors (SVOOA and LVOOA) are characterized by oxygenated ions

274   $C_2H_3O^+$ at m/z 43 and CO_2^+ at m/z 44 respectively. The ratio of most-oxidized ions CO_2^+ (m/z 44)

275   to moderately oxygenated ions $C_2H_3O^+$ (m/z 43) is higher in LVOOA than in SVOOA (Jimenez

276 et al., 2009). Overall, a strong correlation between concentrations of SVOOA and nitrate, a semi-
277 volatile secondary inorganic species, was observed. From November 21st to December 1st
278 (highlighted by the arrow), SVOOA showed distinct peaks beyond the comparable trend with
279 nitrate. The sharp peaks of SVOOA coincide with those of O_3, as shown in the inserted panel.
280 Moreover, higher temperatures were also observed during this period (Fig. S5). LVOOA also
281 correlated well with sulfate in time series as both species are regional pollutants.

282 Fig. 9 shows the monthly average of OA fractions as well as their variations in different ranges of
283 OA concentrations. HOA contributed 23.8% and 28.4% to total OA in November and December
284 respectively. However, HOA increased almost linearly with OA concentration, highlighting the
285 need for traffic control to mitigate high PM concentrations in "buffer" areas. SVOOA and LVOOA
286 remained the dominated OA fractions at OA concentrations below 70 $\mu g/m^3$, which explains the
287 relatively low HOA contribution on a monthly basis.

288

289   Figure 10 shows the diurnal patterns of mass concentrations and fractions for the five OA factors.
290 HOA exhibited two typical peaks during both November and December during the morning rush
291 hour at 09:00 and in the evening around 21:00. HOA accounted for up to 40% of OA (95th
292 percentile of mass fraction in a box-whisker plot) especially in the evening and at night, likely due
293 to heavily polluting trucks passing by *en route* to the city center at night (22:00 to 07:00). These
294 diurnal variations in HOA correspond to those in the H:C ratio and NO_x as well as BC (Fig. S12),
295 further confirming that vehicle-related pollutants are the main contributor to this OA factor.
296 SVOOA had a clear noon-to-afternoon peak in November, consistent with peaks in ozone (Fig.
297 S12), but this peak was less pronounced in December. The noon-to-afternoon peak for SVOOA
298 due to photochemical oxidation processes has been commonly observed worldwide (Hayes et al.,
299 2013; Qin et al., 2016). Zotter et al. (2014) further suggested that the noon-to-afternoon SVOOA
300 peak can be attributed to the large increase in fossil OC. LVOOA showed a relatively flat diurnal
301 pattern, as was found in Shenzhen (He et al., 2011), in contrast to the significant noon-to-afternoon
302 peaks for LVOOA at rural sites in Kaiping (Huang et al., 2011b) and Heshan (Gong et al., 2012).

303 The evolution of AMS OA factors has been used to infer SOA formation via photochemical
304 oxidation in Hong Kong (Lee et al., 2013; Li et al., 2013; Qin et al., 2016b). Fig. 11a shows that
305 SOA (SVOOA+LVOOA) increased as O_x increased during the day (7:00 to 18:00) in both
306 November and December. The SOA concentrations do not show clear correlations with

temperature or liquid water content in aerosols (Fig 11b, 11c). When taken together, these observations suggest that SOA formation in our study was dominated by gas-phase oxidation chemistry rather than heterogeneous or aqueous oxidation pathways. Furthermore, the regression slopes for SOA versus O_x are 0.23 ±0.014 (R_{pr}=0.85) and 0.25 ±0.025 (R_{pr}=0.55) µg /(sm^3 ppb) for November and December respectively. The volume unit "sm" stands for volume under standard-temperature-pressure conditions. The slopes are higher than those reported in earlier studies during spring and summer in North America (Table 2), and significant production of SOA may be attributed to the photo-oxidation of large amounts of accumulated VOCs between the inner city and this peripheral site in Panyu. Liu et al.(2015) investigated SOA formation from light-duty gasoline vehicles operated in China using a smog chamber under idling conditions. They found that SOA formation was 12–259 times higher than POA under conservative OH exposure. Deng et al.(2017) also revealed that the emission factors for BC and POA from major diesel vehicle types in China under idling conditions and the production factor for SOA under photochemical aging were significantly higher than those in studies in Europe and the US and those on light-duty gasoline vehicles in China.

4. Conclusions

   PM pollution in both megacities and their peripheries should be considered together. In this study, we have found that PM_1 levels in Panyu, a peripheral area of Guangzhou, were significantly affected by traffic emissions. OA were the overwhelmingly dominant species (> 45%) at all PM_1 levels. A notable increase in the nitrate-to-sulfate ratio was observed with increases in PM concentration, emphasizing the important role of vehicle emission pollutants on high-PM days.

The formation of total nitrate (particulate + gas) was closely correlated with NO_x during both daytime and nighttime with a much steeper slope during daytime than during nighttime. During the day, total nitrate increased as O_x increased at the same NO_x level, suggesting the photochemical formation of nitrate. At night, high total nitrate concentrations were associated with high NO_x but low O_x levels. Ammonium-rich conditions prevailed throughout the campaign and particulate nitrate was closely associated with excess ammonium. The fraction of particle phase nitrate in December was higher than that in November, primarily due to lower temperatures that favored the partitioning of nitrate toward particle phase.

338 The nighttime emissions of OA and efficient photochemical production of SOA during the day
339 together accounted for continued high OA concentrations. HOA increased almost linearly with
340 OA concentration and contributed up to 40% of the high organic concentrations at night. SOA
341 (SVOOA+LVOOA) played a more important role on monthly averages and during the day. SOA
342 concentrations changed with the photochemical oxidation marker (O_x), and the observed ratios of
343 SOA to O_x were higher than those reported for Pasadena and Mexico City during the summer. This
344 efficient SOA formation was fueled by large sources of SOA precursors (e.g. HOA and VOCs) on
345 the periphery of Guangzhou. PM pollution in both megacities and their peripheries should thus be
346 considered together.
347

348 **5. Acknowledgements:**
349
350 This work was supported by the National Key Project of the Ministry of Science and Technology
351 of the People's Republic of China (2016YFC0201901) and the National Natural Science
352 Foundation of China (41375156). We also thank Dr. Mai Boru for providing CO_2 data. Yi Ming
353 Qin gratefully acknowledges support from the HKUST Asian Future Leaders Scholarship.
354

355 **6. References:**

356 Aiken, A. C., DeCarlo, P. F. and Jimenez, J. L.: Elemental analysis of organic species with
357 electron ionization high-resolution mass spectrometry., Anal. Chem., 79(21), 8350–8,
358 doi:10.1021/ac071150w, 2007.

359 Aiken, A. C., Salcedo, D., Cubison, M. J., Huffman, J. A., DeCarlo, P. F., Ulbrich, I. M.,
360 Docherty, K. S., Sueper, D., Kimmel, J. R., Worsnop, D. R., Trimborn, A., Northway, M., Stone,
361 E. A., Schauer, J. J., Volkamer, R. M., Fortner, E., de Foy, B., Wang, J., Laskin, A.,
362 Shutthanandan, V., Zheng, J., Zhang, R., Gaffney, J., Marley, N. A., Paredes-Miranda, G.,
363 Arnott, W. P., Molina, L. T., Sosa, G. and Jimenez, J. L.: Mexico City aerosol analysis during
364 MILAGRO using high resolution aerosol mass spectrometry at the urban supersite (T0) – Part 1:
365 Fine particle composition and organic source apportionment, Atmos. Chem. Phys., 9(17), 6633–
366 6653, doi:10.5194/acp-9-6633-2009, 2009.

367 Alfarra, M. R., Prevot, A. S. H., Szidat, S., Sandradewi, J., Weimer, S., Lanz, V. A., Schreiber,
368 D., Martin Mohr, A. and Urs, B.: Identification of the Mass Spectral Signature of Organic
369 Aerosols from Wood Burning Emissions, , doi:10.1021/ES062289B, 2007.

370 Arimoto, R.: Arimoto et al., 1996.pdf, J. Geophys. Res., 101(d1), 2011–2023,
371 doi:10.1029/95JD01071, 1996.

372 Canagaratna, M. R., Jimenez, J. L., Kroll, J. H., Chen, Q., Kessler, S. H., Massoli, P.,
373 Hildebrandt Ruiz, L., Fortner, E., Williams, L. R., Wilson, K. R., Surratt, J. D., Donahue, N. M.,
374 Jayne, J. T. and Worsnop, D. R.: Elemental ratio measurements of organic compounds using
375 aerosol mass spectrometry: characterization, improved calibration, and implications, Atmos.
376 Chem. Phys., 15(1), 253–272, doi:10.5194/acp-15-253-2015, 2015.

377 Canonaco, F., Crippa, M., Slowik, J. G., Baltensperger, U. and Prévôt, A. S. H.: SoFi, an IGOR-
378 based interface for the efficient use of the generalized multilinear engine (ME-2) for the source
379 apportionment: ME-2 application to aerosol mass spectrometer data, Atmos. Meas. Tech., 6(12),
380 3649–3661, doi:10.5194/amt-6-3649-2013, 2013.

381 Chan, C. K. and Yao, X.: Air pollution in mega cities in China, Atmos. Environ., 42(1), 1–42,
382 doi:10.1016/j.atmosenv.2007.09.003, 2008.

383 Clegg, S. L., Brimblecombe, P. and Wexler, A. S.: Thermodynamic Model of the System H^+
384 $-NH_4^+ -Na^+ -SO_4^{2-} -NO_3^- -Cl^- -H_2O$ at 298.15 K, J. Phys. Chem. A, 102(12), 2155–
385 2171, doi:10.1021/jp973043j, 1998.

386 Crippa, M., Canonaco, F., Lanz, V. A., Äijälä, M., Allan, J. D., Carbone, S., Capes, G., Ceburnis,
387 D., Dall'Osto, M., Day, D. A., DeCarlo, P. F., Ehn, M., Eriksson, A., Freney, E., Hildebrandt
388 Ruiz, L., Hillamo, R., Jimenez, J. L., Junninen, H., Kiendler-Scharr, A., Kortelainen, A.-M.,
389 Kulmala, M., Laaksonen, A., Mensah, A. A., Mohr, C., Nemitz, E., O'Dowd, C., Ovadnevaite,
390 J., Pandis, S. N., Petäjä, T., Poulain, L., Saarikoski, S., Sellegri, K., Swietlicki, E., Tiitta, P.,
391 Worsnop, D. R., Baltensperger, U. and Prévôt, A. S. H.: Organic aerosol components derived
392 from 25 AMS data sets across Europe using a consistent ME-2 based source apportionment
393 approach, Atmos. Chem. Phys., 14(12), 6159–6176, doi:10.5194/acp-14-6159-2014, 2014.

394 Decarlo, P. F., Kimmel, J. R., Trimborn, A., Northway, M. J., Jayne, J. T., Aiken, A. C., Gonin,
395 M., Fuhrer, K., Horvath, T., Docherty, K. S., Worsnop, D. R. and Jimenez, J. L.: Field-
396 Deployable, High-Resolution, Time-of-Flight Aerosol Mass Spectrometer, Anal. Chem., 78(24),
397 8281–8289, doi:8410.1029/2001JD001213.Analytical, 2006.

398 Deng, W., Hu, Q., Liu, T., Wang, X., Zhang, Y., Song, W., Sun, Y., Bi, X., Yu, J., Yang, W.,
399 Huang, X., Zhang, Z., Huang, Z., He, Q., Mellouki, A. and George, C.: Primary particulate
400 emissions and secondary organic aerosol (SOA) formation from idling diesel vehicle exhaust in

China, Sci. Total Environ., 593, 462–469, doi:10.1016/j.scitotenv.2017.03.088, 2017.

Docherty, K. S., Aiken, A. C., Huffman, J. A., Ulbrich, I. M., Decarlo, P. F., Sueper, D., Worsnop, D. R., Snyder, D. C., Peltier, R. E., Weber, R. J., Grover, B. D., Eatough, D. J., Williams, B. J., Goldstein, A. H., Ziemann, P. J. and Jimenez, J. L.: The 2005 Study of Organic Aerosols at Riverside (SOAR-1): Instrumental intercomparisons and fine particle composition, Atmos. Chem. Phys., 11(23), 12387–12420, doi:10.5194/acp-11-12387-2011, 2011.

Drinovec, L., Močnik, G., Zotter, P., Prévôt, A. S. H., Ruckstuhl, C., Coz, E., Rupakheti, M., Sciare, J., Müller, T., Wiedensohler, A. and Hansen, A. D. A.: The "dual-spot" Aethalometer: An improved measurement of aerosol black carbon with real-time loading compensation, Atmos. Meas. Tech., 8(5), 1965–1979, doi:10.5194/amt-8-1965-2015, 2015.

Elser, M., Huang, R.-J., Wolf, R., Slowik, J. G., Wang, Q., Canonaco, F., Li, G., Bozzetti, C., Daellenbach, K. R., Huang, Y., Zhang, R., Li, Z., Cao, J., Baltensperger, U., El-Haddad, I. and Prévôt, A. S. H.: New insights into PM_{2.5} chemical composition and sources in two major cities in China during extreme haze events using aerosol mass spectrometry, Atmos. Chem. Phys., 16(5), 3207–3225, doi:10.5194/acp-16-3207-2016, 2016.

Farmer, D. K., Matsunaga, a, Docherty, K. S., Surratt, J. D., Seinfeld, J. H., Ziemann, P. J. and Jimenez, J. L.: Response of an aerosol mass spectrometer to organonitrates and organosulfates and implications for atmospheric chemistry., Proc. Natl. Acad. Sci. U. S. A., 107(15), 6670–6675, doi:10.1073/pnas.0912340107, 2010.

Fröhlich, R., Crenn, V., Setyan, A., Belis, C. A., Canonaco, F., Favez, O., Riffault, V., Slowik, J. G., Aas, W., Aijälä, M., Alastuey, A., Artiñano, B., Bonnaire, N., Bozzetti, C., Bressi, M., Carbone, C., Coz, E., Croteau, P. L., Cubison, M. J., Esser-Gietl, J. K., Green, D. C., Gros, V., Heikkinen, L., Herrmann, H., Jayne, J. T., Lunder, C. R., Minguillón, M. C., Močnik, G., O'Dowd, C. D., Ovadnevaite, J., Petralia, E., Poulain, L., Priestman, M., Ripoll, A., Sarda-Estève, R., Wiedensohler, A., Baltensperger, U., Sciare, J. and Prévôt, A. S. H.: ACTRIS ACSM intercomparison – Part 2: Intercomparison of ME-2 organic source apportionment results from 15 individual, co-located aerosol mass spectrometers, Atmos. Meas. Tech., 8(6), 2555–2576, doi:10.5194/amt-8-2555-2015, 2015.

Gentner, D. R., Jathar, S. H., Gordon, T. D., Bahreini, R., Day, D. A., El Haddad, I., Hayes, P. L., Pieber, S. M., Platt, S. M., de Gouw, J., Goldstein, A. H., Harley, R. A., Jimenez, J. L., Prévôt, A. S. H. and Robinson, A. L.: Review of Urban Secondary Organic Aerosol Formation from Gasoline and Diesel Motor Vehicle Emissions, Environ. Sci. Technol., 51(3), 1074–1093, doi:10.1021/acs.est.6b04509, 2017.

Gong, Z., Lan, Z., Xue, L., Zeng, L., He, L. and Huang, X.: Characterization of submicron aerosols in the urban outflow of the central Pearl River Delta region of China, Front. Environ. Sci. Eng. China, 6(5), 725–733, doi:10.1007/s11783-012-0441-8, 2012.

Griffith, S. M., Huang, X. H. H. H., Louie, P. K. K. K. K. and Yu, J. Z.: Characterizing the thermodynamic and chemical composition factors controlling PM2.5 nitrate: Insights gained from two years of online measurements in Hong Kong, Atmos. Environ., 122, 864–875, doi:10.1016/j.atmosenv.2015.02.009, 2015.

Hayes, P. L., Ortega, a. M., Cubison, M. J., Froyd, K. D., Zhao, Y., Cliff, S. S., Hu, W. W., Toohey, D. W., Flynn, J. H., Lefer, B. L., Grossberg, N., Alvarez, S., Rappenglück, B., Taylor, J. W., Allan, J. D., Holloway, J. S., Gilman, J. B., Kuster, W. C., De Gouw, J. a., Massoli, P., Zhang, X., Liu, J., Weber, R. J., Corrigan, a. L., Russell, L. M., Isaacman, G., Worton, D. R., Kreisberg, N. M., Goldstein, a. H., Thalman, R., Waxman, E. M., Volkamer, R., Lin, Y. H., Surratt, J. D., Kleindienst, T. E., Offenberg, J. H., Dusanter, S., Griffith, S., Stevens, P. S.,

447   Brioude, J., Angevine, W. M. and Jimenez, J. L.: Organic aerosol composition and sources in
448   Pasadena, California, during the 2010 CalNex campaign, J. Geophys. Res. Atmos., 118(16),
449   9233–9257, doi:10.1002/jgrd.50530, 2013.
450   He, L.-Y., Huang, X.-F., Xue, L., Hu, M., Lin, Y., Zheng, J., Zhang, R. and Zhang, Y.-H.:
451   Submicron aerosol analysis and organic source apportionment in an urban atmosphere in Pearl
452   River Delta of China using high-resolution aerosol mass spectrometry, J. Geophys. Res.,
453   116(D12), D12304, doi:10.1029/2010JD014566, 2011.
454   He, L. Y., Lin, Y., Huang, X. F., Guo, S., Xue, L., Su, Q., Hu, M., Luan, S. J. and Zhang, Y. H.:
455   Characterization of high-resolution aerosol mass spectra of primary organic aerosol emissions
456   from Chinese cooking and biomass burning, Atmos. Chem. Phys., 10(23), 11535–11543,
457   doi:10.5194/acp-10-11535-2010, 2010.
458   Ho, K. ., Lee, S. ., Chan, C. K., Yu, J. C., Chow, J. C. and Yao, X. .: Characterization of
459   chemical species in PM2.5 and PM10 aerosols in Hong Kong, Atmos. Environ., 37(1), 31–39,
460   doi:10.1016/S1352-2310(02)00804-X, 2003.
461   Hu, W. W., Hu, M., Yuan, B., Jimenez, J. L., Tang, Q., Peng, J. F., Hu, W. W., Shao, M., Wang,
462   M., Zeng, L. M., Wu, Y. S., Gong, Z. H., Huang, X. F. and He, L. Y.: Insights on organic aerosol
463   aging and the influence of coal combustion at a regional receptor site of central eastern China,
464   Atmos. Chem. Phys., 13(19), 10095–10112, doi:10.5194/acp-13-10095-2013, 2013.
465   Huang, X., He, L., Hu, M., Canagaratna, M. R., Sun, Y., Zhang, Q., Zhu, T., Xue, L., Zeng, L.
466   and Liu, X.: and Physics Highly time-resolved chemical characterization of atmospheric
467   submicron particles during 2008 Beijing Olympic Games using an Aerodyne High-Resolution
468   Aerosol Mass Spectrometer, , 8933–8945, doi:10.5194/acp-10-8933-2010, 2010.
469   Huang, X., Qiu, R., Chan, C. K. and Ravi Kant, P.: Evidence of high PM2.5 strong acidity in
470   ammonia-rich atmosphere of Guangzhou, China: Transition in pathways of ambient ammonia to
471   form aerosol ammonium at [NH4+]/[SO42-]=1.5, Atmos. Res., 99(3–4), 488–495,
472   doi:10.1016/j.atmosres.2010.11.021, 2011a.
473   Huang, X.-F. F., He, L.-Y. Y., Hu, M., Canagaratna, M. R., Kroll, J. H., Ng, N. L., Zhang, Y.-H.
474   H., Lin, Y., Xue, L., Sun, T.-L. L., Liu, X.-G. G., Shao, M., Jayne, J. T. and Worsnop, D. R.:
475   Characterization of submicron aerosols at a rural site in Pearl River Delta of China using an
476   Aerodyne High-Resolution Aerosol Mass Spectrometer, Atmos. Chem. Phys., 11(5), 1865–1877,
477   doi:10.5194/acp-11-1865-2011, 2011b.
478   Jimenez, J. L., Canagaratna, M. R., Donahue, N. M., Prevot, a S. H., Zhang, Q., Kroll, J. H.,
479   DeCarlo, P. F., Allan, J. D., Coe, H., Ng, N. L., Aiken, a C., Docherty, K. S., Ulbrich, I. M.,
480   Grieshop, a P., Robinson, a L., Duplissy, J., Smith, J. D., Wilson, K. R., Lanz, V. a, Hueglin,
481   C., Sun, Y. L., Tian, J., Laaksonen, a, Raatikainen, T., Rautiainen, J., Vaattovaara, P., Ehn, M.,
482   Kulmala, M., Tomlinson, J. M., Collins, D. R., Cubison, M. J., Dunlea, E. J., Huffman, J. a,
483   Onasch, T. B., Alfarra, M. R., Williams, P. I., Bower, K., Kondo, Y., Schneider, J., Drewnick, F.,
484   Borrmann, S., Weimer, S., Demerjian, K., Salcedo, D., Cottrell, L., Griffin, R., Takami, a,
485   Miyoshi, T., Hatakeyama, S., Shimono, a, Sun, J. Y., Zhang, Y. M., Dzepina, K., Kimmel, J. R.,
486   Sueper, D., Jayne, J. T., Herndon, S. C., Trimborn, a M., Williams, L. R., Wood, E. C.,
487   Middlebrook, a M., Kolb, C. E., Baltensperger, U. and Worsnop, D. R.: Evolution of organic
488   aerosols in the atmosphere., Science, 326(5959), 1525–1529, doi:10.1126/science.1180353,
489   2009.
490   Kelly, F. J. and Zhu, T.: Transport solutions for cleaner air, Science (80-.)., 352(6288), 934–936,
491   doi:10.1126/science.aaf3420, 2016.
492   Lee, B. P., Li, Y. J., Yu, J. Z., Louie, P. K. K. and Chan, C. K.: Physical and chemical

493   characterization of ambient aerosol by HR-ToF-AMS at a suburban site in Hong Kong during
494   springtime 2011, J. Geophys. Res. Atmos., 118(15), 8625–8639, doi:10.1002/jgrd.50658, 2013.
495   Lee, B. P., Li, Y. J., Yu, J. Z., Louie, P. K. K. and Chan, C. K.: Journal of Geophysical
496   Research : Atmospheres, , 1–19, doi:10.1002/2015JD023311.Received, 2015.
497   Li, Y. J., Lee, B. Y. L., Yu, J. Z., Ng, N. L. and Chan, C. K.: Evaluating the degree of
498   oxygenation of organic aerosol during foggy and hazy days in Hong Kong using high-resolution
499   time-of-flight aerosol mass spectrometry (HR-ToF-AMS), Atmos. Chem. Phys., 13(17), 8739–
500   8753, doi:10.5194/acp-13-8739-2013, 2013.
501   Li, Y. J., Sun, Y., Zhang, Q., Li, X., Li, M., Zhou, Z. and Chan, C. K.: Real-time chemical
502   characterization of atmospheric particulate matter in China : A review, Atmos. Environ., 158,
503   270–304, doi:10.1016/j.atmosenv.2017.02.027, 2017.
504   Liu, T., Wang, X., Deng, W., Hu, Q., Ding, X., Zhang, Y., He, Q., Zhang, Z., L??, S., Bi, X.,
505   Chen, J. and Yu, J.: Secondary organic aerosol formation from photochemical aging of light-duty
506   gasoline vehicle exhausts in a smog chamber, Atmos. Chem. Phys., 15(15), 9049–9062,
507   doi:10.5194/acp-15-9049-2015, 2015a.
508   Liu, X., Sun, K., Qu, Y., Hu, M., Sun, Y., Zhang, F. and Zhang, Y.: Secondary formation of
509   sulfate and nitrate during a haze episode in megacity beijing, china, Aerosol Air Qual. Res.,
510   15(6), 2246–2257, doi:10.4209/aaqr.2014.12.0321, 2015b.
511   Louie, P. K. K., Chow, J. C., Chen, L. W. A., Watson, J. G., Leung, G. and Sin, D. W. M.:
512   PM2.5 chemical composition in Hong Kong: Urban and regional variations, Sci. Total Environ.,
513   338(3), 267–281, doi:10.1016/j.scitotenv.2004.07.021, 2005.
514   Middlebrook, A. M., Bahreini, R., Jimenez, J. L. and Canagaratna, M. R.: Evaluation of
515   Composition-Dependent Collection Efficiencies for the Aerodyne Aerosol Mass Spectrometer
516   using Field Data, Aerosol Sci. Technol., 46(3), 258–271, doi:10.1080/02786826.2011.620041,
517   2012.
518   Mohr, C., DeCarlo, P. F., Heringa, M. F., Chirico, R., Slowik, J. G., Richter, R., Reche, C.,
519   Alastuey, A., Querol, X., Seco, R., Peñuelas, J., Jiménez, J. L., Crippa, M., Zimmermann, R.,
520   Baltensperger, U. and Prévôt, A. S. H.: Identification and quantification of organic aerosol from
521   cooking and other sources in Barcelona using aerosol mass spectrometer data, Atmos. Chem.
522   Phys., 12(4), 1649–1665, doi:10.5194/acp-12-1649-2012, 2012.
523   Paatero, P. and Hopke, P. K.: Rotational tools for factor analytic models, J. Chemom., 23(2), 91–
524   100, doi:10.1002/cem.1197, 2009.
525   Pan, Y., Wang, Y., Zhang, J., Liu, Z., Wang, L., Tian, S., Tang, G., Gao, W., Ji, D., Song, T. and
526   Wang, Y.: Redefining the importance of nitrate during haze pollution to help optimize an
527   emission control strategy., 2016.
528   Pathak, R. K., Louie, P. K. K. and Chan, C. K.: Characteristics of aerosol acidity in Hong Kong,
529   Atmos. Environ., 38(19), 2965–2974, doi:10.1016/j.atmosenv.2004.02.044, 2004.
530   Platt, S. M., El Haddad, I., Pieber, S. M., Huang, R.-J., Zardini, A. A., Clairotte, M., Suarez-
531   Bertoa, R., Barmet, P., Pfaffenberger, L., Wolf, R., Slowik, J. G., Fuller, S. J., Kalberer, M.,
532   Chirico, R., Dommen, J., Astorga, C., Zimmermann, R., Marchand, N., Hellebust, S., Temime-
533   Roussel, B., Baltensperger, U. and Prévôt, A. S. H.: Two-stroke scooters are a dominant source
534   of air pollution in many cities., Nat. Commun., 5(May), 3749, doi:10.1038/ncomms4749, 2014.
535   Qin, Y. M., Li, Y. J., Wang, H., Lee, B. P. Y. L., Huang, D. D. and Chan, C. K.: Particulate
536   matter (PM) episodes at a suburban site in Hong Kong: evolution of PM characteristics and role
537   of photochemistry in secondary aerosol formation, Atmos. Chem. Phys. Discuss., 0, 1–32,
538   doi:10.5194/acp-2016-414, 2016a.

539   Qin, Y. M., Li, Y. J., Wang, H., Lee, B. P. Y. L., Huang, D. D. and Chan, C. K.: Particulate
540   matter (PM) episodes at a suburban site in Hong Kong: evolution of PM characteristics and role
541   of photochemistry in secondary aerosol formation, Atmos. Chem. Phys., 16(11), 14131–14145,
542   doi:10.5194/acp-2016-414, 2016b.
543   Schneider, J., Weimer, S., Drewnick, F., Borrmann, S., Helas, G., Gwaze, P., Schmid, O.,
544   Andreae, M. O. and Kirchner, U.: Mass spectrometric analysis and aerodynamic properties of
545   various types of combustion-related aerosol particles, Int. J. Mass Spectrom., 258(1–3), 37–49,
546   doi:10.1016/j.ijms.2006.07.008, 2006.
547   Schurman, M. I., Lee, T., Sun, Y., Schichtel, B. A., Kreidenweis, S. M. and Collett Jr., J. L.:
548   Investigating types and sources of organic aerosol in Rocky Mountain National Park using
549   aerosol mass spectrometry, Atmos. Chem. Phys., 15(2), 737–752, doi:10.5194/acp-15-737-2015,
550   2015a.
551   Schurman, M. I., Lee, T., Desyaterik, Y., Schichtel, B. A., Kreidenweis, S. M. and Collett, J. L.:
552   Transport, biomass burning, and in-situ formation contribute to fine particle concentrations at a
553   remote site near Grand Teton National Park, Atmos. Environ., 112, 257–268,
554   doi:10.1016/j.atmosenv.2015.04.043, 2015b.
555   Seinfeld, J. H. and Pandis, S. N.: ATMOSPHERIC From Air Pollution to Climate Change
556   SECOND EDITION., 2006.
557   Sun, Y. L., Zhang, Q., Schwab, J. J., Demerjian, K. L., Chen, W. N., Bae, M. S., Hung, H. M.,
558   Hogrefe, O., Frank, B., Rattigan, O. V. and Lin, Y. C.: Characterization of the sources and
559   processes of organic and inorganic aerosols in New York city with a high-resolution time-of-
560   flight aerosol mass apectrometer, Atmos. Chem. Phys., 11(4), 1581–1602, doi:10.5194/acp-11-
561   1581-2011, 2011.
562   Tan, H., Yin, Y., Gu, X., Li, F., Chan, P. W., Xu, H., Deng, X. and Wan, Q.: An observational
563   study of the hygroscopic properties of aerosols over the Pearl River Delta region, Atmos.
564   Environ., 77, 817–826, doi:10.1016/j.atmosenv.2013.05.049, 2013.
565   Tan, J. H., Duan, J. C., Chen, D. H., Wang, X. H., Guo, S. J., Bi, X. H., Sheng, G. Y., He, K. Bin
566   and Fu, J. M.: Chemical characteristics of haze during summer and winter in Guangzhou, Atmos.
567   Res., 94(2), 238–245, doi:10.1016/j.atmosres.2009.05.016, 2009.
568   Wang, Y., Zhang, Q. Q., He, K., Zhang, Q. and Chai, L.: Sulfate-nitrate-ammonium aerosols
569   over China: Response to 2000-2015 emission changes of sulfur dioxide, nitrogen oxides, and
570   ammonia, Atmos. Chem. Phys., 13(5), 2635–2652, doi:10.5194/acp-13-2635-2013, 2013.
571   Wen, L., Chen, J., Yang, L., Wang, X., Xu, C., Sui, X., Yao, L., Zhu, Y., Zhang, J., Zhu, T. and
572   Wang, W.: Enhanced formation of fine particulate nitrate at a rural site on the North China Plain
573   in summer: The important roles of ammonia and ozone, Atmos. Environ., 101, 294–302,
574   doi:10.1016/j.atmosenv.2014.11.037, 2015.
575   Wu, X., Wu, Y., Zhang, S., Liu, H., Fu, L. and Hao, J.: Assessment of vehicle emission
576   programs in China during 1998-2013: Achievement, challenges and implications, Environ.
577   Pollut., 214(X), 556–567, doi:10.1016/j.envpol.2016.04.042, 2016.
578   Xu, L., Suresh, S., Guo, H., Weber, R. J. and Ng, N. L.: Aerosol characterization over the
579   southeastern United States using high-resolution aerosol mass spectrometry: spatial and seasonal
580   variation of aerosol composition and sources with a focus on organic nitrates, Atmos. Chem.
581   Phys., 15(13), 7307–7336, doi:10.5194/acp-15-7307-2015, 2015.
582   Xue, J., Yuan, Z., Lau, A. K. H. and Yu, J. Z.: Insights into factors affecting nitrate in $PM_{2.5}$ in a
583   polluted high NO_x environment through hourly observations and size distribution
584   measurements, J. Geophys. Res. Atmos., 119(8), 4888–4902, doi:10.1002/2013JD021108, 2014.

585   Zhang, Q., Geng, G. N., Wang, S. W., Richter, A. and He, K. Bin: Satellite remote sensing of
586   changes in NO x emissions over China during 1996-2010, Chinese Sci. Bull., 57(22), 2857–
587   2864, doi:10.1007/s11434-012-5015-4, 2012.
588   Zhang, R., Wang, G., Guo, S., Zamora, M. L., Ying, Q., Lin, Y., Wang, W., Hu, M. and Wang,
589   Y.: Formation of Urban Fine Particulate Matter, Chem. Rev., 115(10), 3803–3855,
590   doi:10.1021/acs.chemrev.5b00067, 2015.
591   Zhang, Y., Cai, J., Wang, S., He, K. and Zheng, M.: Review of receptor-based source
592   apportionment research of fine particulate matter and its challenges in China, Sci. Total Environ.,
593   586, 917–929, doi:10.1016/j.scitotenv.2017.02.071, 2017.
594   Zhang, Y.-L. and Cao, F.: Fine particulate matter (PM 2.5) in China at a city level., Sci. Rep., 5,
595   14884, doi:10.1038/srep14884, 2015.
596   Zotter, P., El-haddad, I., Zhang, Y., Hayes, P. L., Zhang, X., Lin, Y., Wacker, L., Schnelle-kreis,
597   J., Abbaszade, G., Zimmermann, R., Surratt, J. D., Weber, R., Jimenez, J. L., Szidat, S.,
598   Baltensperger, U. and Prévôt, A. S. H.: Journal of Geophysical Research : Atmospheres, , 1–18,
599   doi:10.1002/2013JD021114.Received, 2014.
600   Zou, Y., Deng, X. J., Zhu, D., Gong, D. C., Wang, H., Li, F., Tan, H. B., Deng, T., Mai, B. R.,
601   Liu, X. T. and Wang, B. G.: Characteristics of 1 year of observational data of VOCs, NO_x and O_3
602   at a suburban site in Guangzhou, China, Atmos. Chem. Phys., 15(12), 6625–6636,
603   doi:10.5194/acp-15-6625-2015, 2015.
604

Table 1. Elemental ratios of organic PM$_1$ in the PRD

Site/characteristics	Month	Aiken-Ambient (A-A) method			Improved-Ambient (I-A) method			Reference
		O:C	**H:C**	**OM:OC**	**O:C***	**H:C***	**OM:OC***	
Panyu/suburban	November	0.42	1.49	1.71	0.53	1.63	1.87	This study
	December	0.41	1.5	1.70	0.53	1.65	1.87	
Kaiping/rural	November	0.47	1.48	1.77	0.60[*]	1.64[*]	1.94[*]	Huang et al., 2011
Shenzhen/urban	November	0.3	1.63	1.57	0.38[*]	1.81[*]	1.66[*]	He et al., 2011
Heshan/rural	November	0.4	1.49	1.72	0.51[*]	1.65[*]	1.83[*]	Gong et al., 2012
HKUST/suburban	February	0.42	1.39	1.71	0.53[*]	1.54[*]	1.86[*]	Li et al., 2015
	December	0.43	1.4	1.71	0.55[*]	1.55[*]	1.87[*]	
Mong Kok/urban	March-mid May	0.25	1.68	1.49	0.32	1.84	1.59	Lee et al., 2015

* Improved-Ambient elemental ratios were estimated using the A-A method with empirical constants from M. R. Canagaratna et al. (2015).

Table 2. Comparison of SOA-O_x average ratios

Site	Month	Season	SOA-Ox average ratio	Reference
Panyu, Guangzhou	November	Late autumn	0.23 μg /(sm^3 ppb) [*]	This study
	December	Winter	0.25 μg /(sm^3 ppb) [*]	
Pasadena, CA	May-June (morning)	Late spring-summer	0.183 μg /(sm^3 ppb) [*]	Hayes et al., 2013
	May-June (afternoon)	Late spring-summer	0.163 μg /(sm^3 ppb) [*]	
Riverside, CA	July-August	summer	0.142 μg /(sm^3 ppb) [*]	Docherty et al., 2011
Mexico City	March	spring	0.156 μg /(sm^3 ppb) [*]	Aiken et al., 2009
New York City	July	summer	0.12 μg /(sm^3 ppb)	Sun et al., 2011

[*]The volume unit "sm" stands for volume under standard-temperature-pressure conditions.

Organics sulfate ammonium nitrate Chloride black carbon
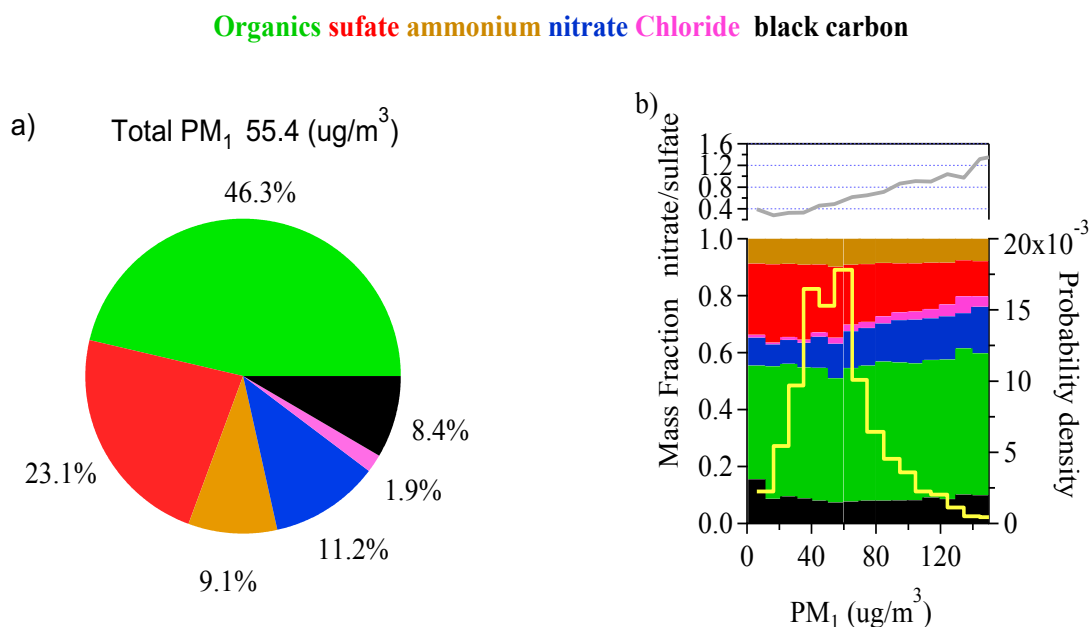
Figure 1. a) Average mass fraction of PM$_1$ (with BC inclusive) throughout the entire campaign; b) Mass fraction variation among PM$_1$ species, nitrate to sulfate mass ratio as well as the probability density of PM$_1$ as a function of total PM$_1$ mass loading. The probability density distribution describes the relative likelihood of PM$_1$ mass loading in a range of concentrations.
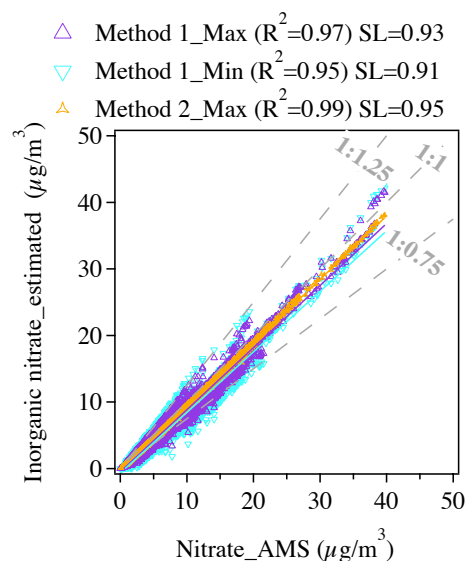
Figure 2. Scatter plot of estimated inorganic nitrate versa nitrate from HR-ToF-AMS measurement. SL denotes the slope for the linear regression fitting.
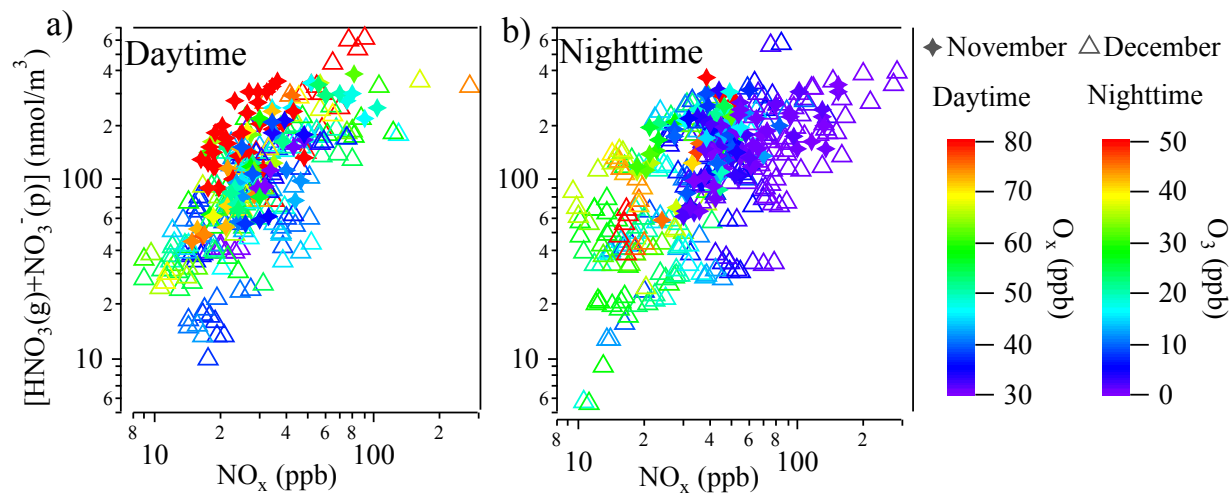
Figure 3. Correlations between total nitrate (HNO$_3$(g)+ NO3(p)) and NO$_x$ (NO+NO$_2$). Triangles and circles represent data for November and December respectively. Data are color-coded by O$_x$ during the day and O$_3$ at night.
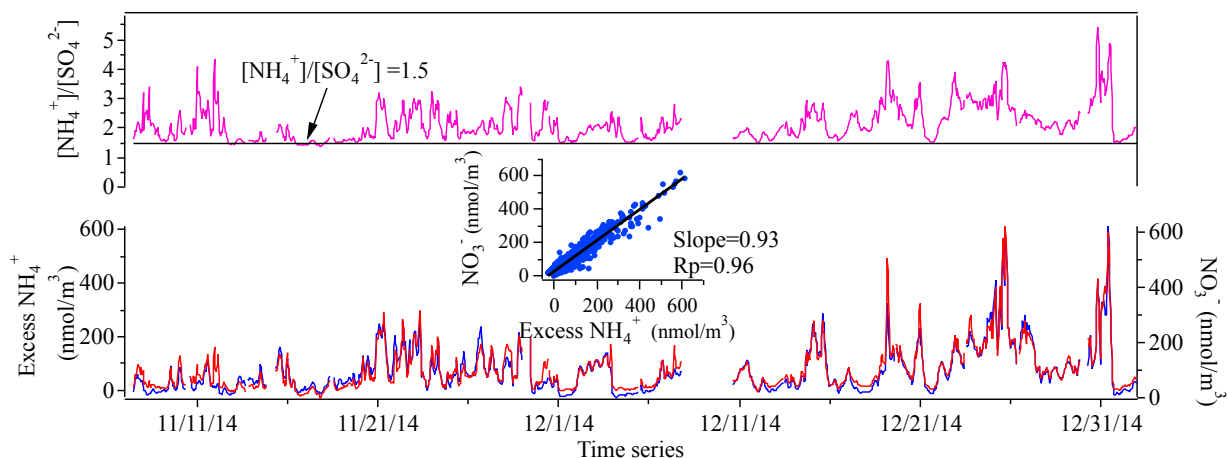
Figure 4. Time series of nitrate, excess ammonium and ammonium-to-sulfate molar ratio.
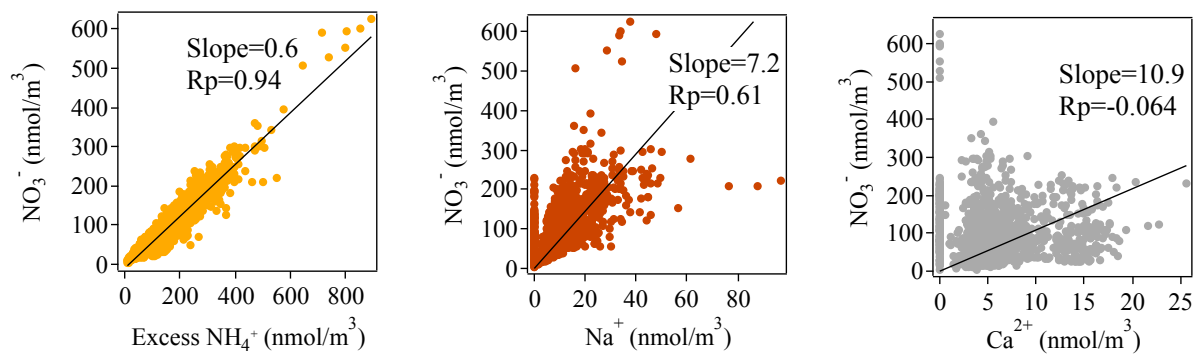
Figure 5. Scatter plots of NO$_3^-$ molar concentration from MARGA (PM$_{2.5}$) against those of excess NH$_4^+$, Na$^+$ and Ca^{2+}.
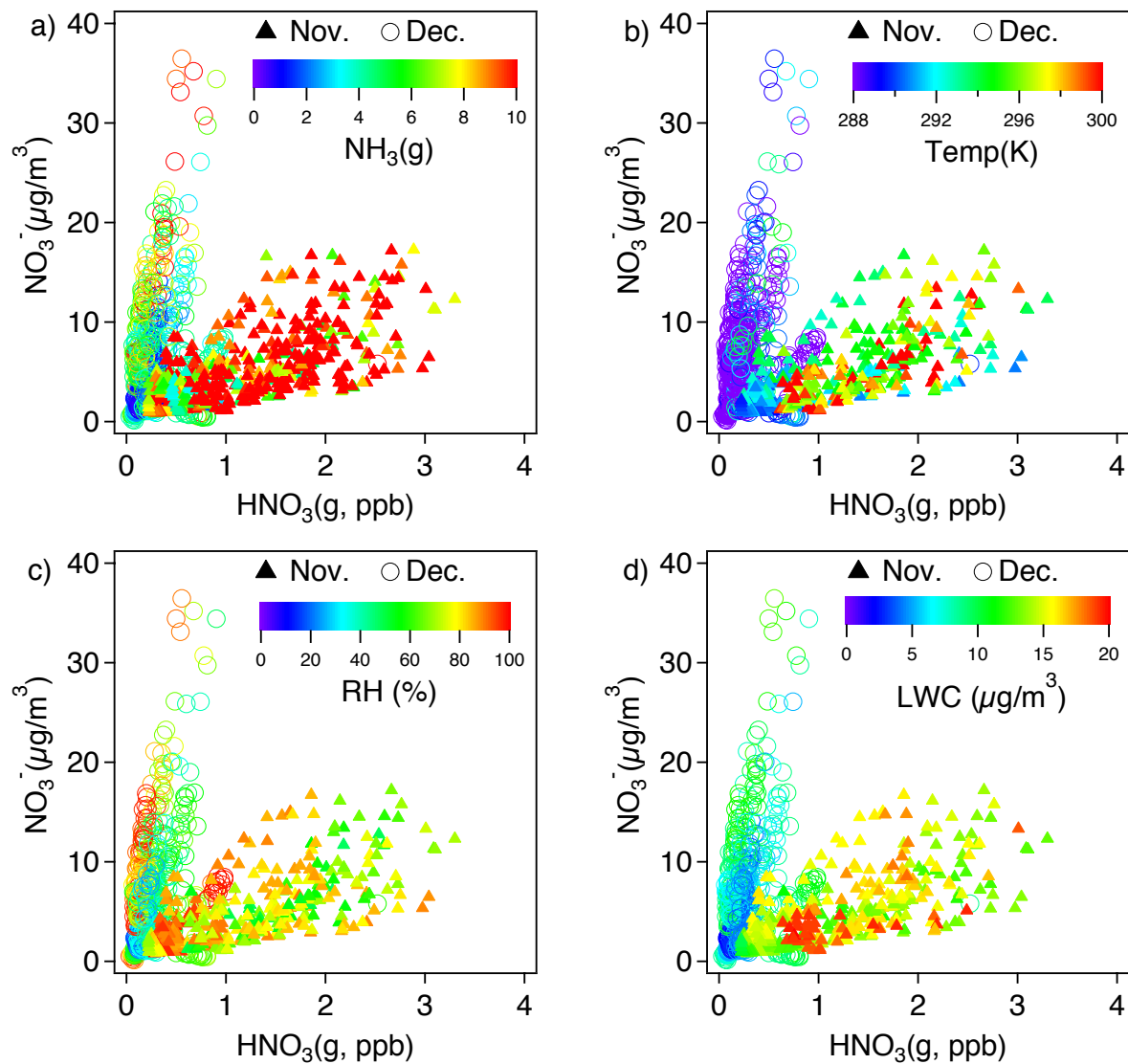
Figure 6. Distribution of nitrate species between HNO$_3$(g) and NO$_3^-$(p), colored by (a)NH$_3$ concentration (b) temperature, (c) RH, and (d) LWC.
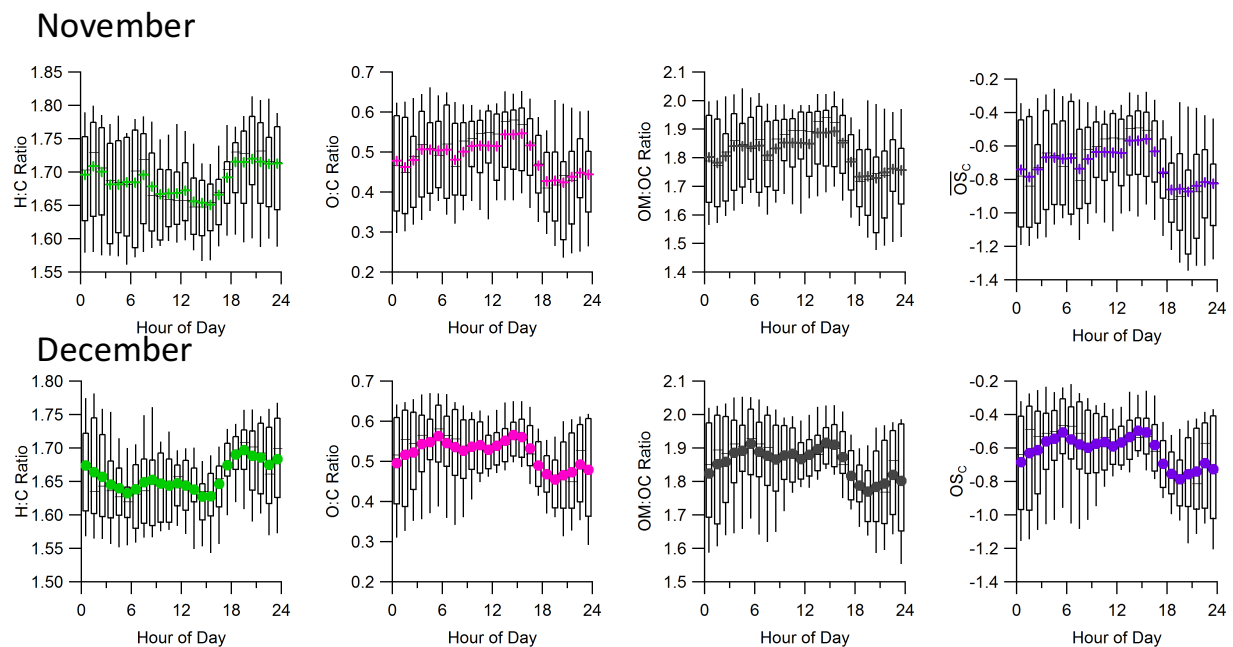
Figure 7. Diurnal variations in H:C, O:C, and OM:OC ratios and carbon oxidation state ($\overline{OS}_c \approx$ 2×O:C-H:C) during Nov. and Dec. (25th and 75th percentile boxes, 5th and 95th percentile whiskers, median as line in box, and mean as solid colored line).
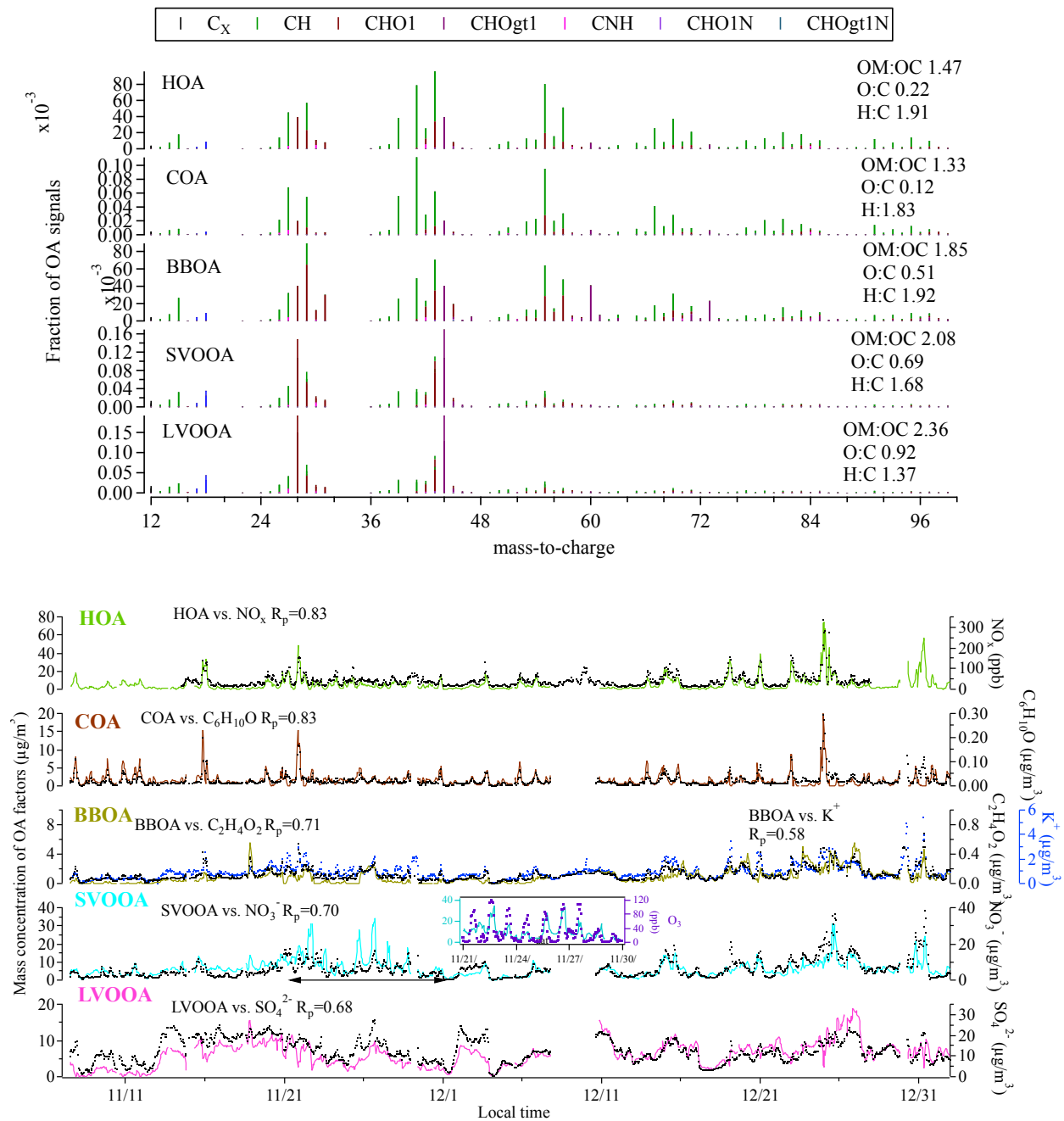
Figure. 8. The mass spectra of all OA factors and the time series of their mass concentrations together with external tracers.
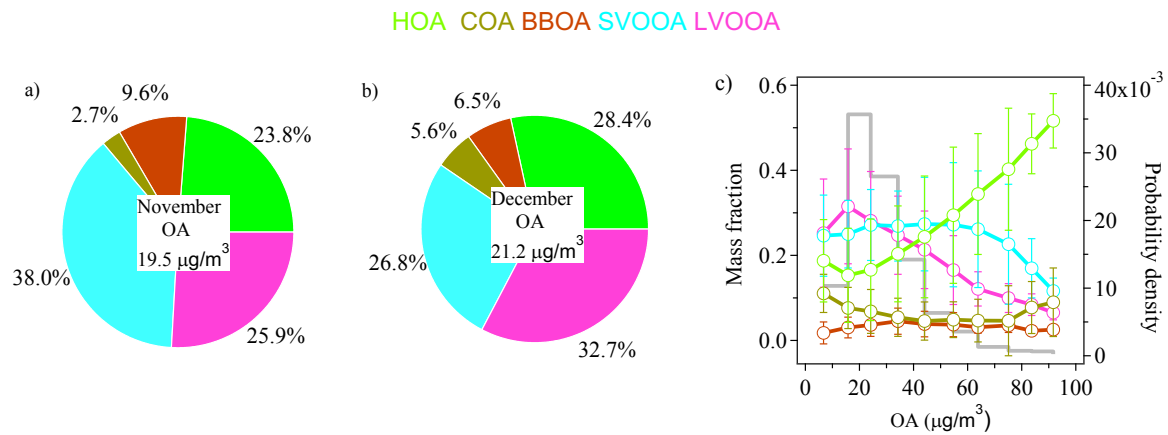
Figure 9. Monthly averages of OA fraction as well as variations in OA fractions in different ranges of OA concentration.
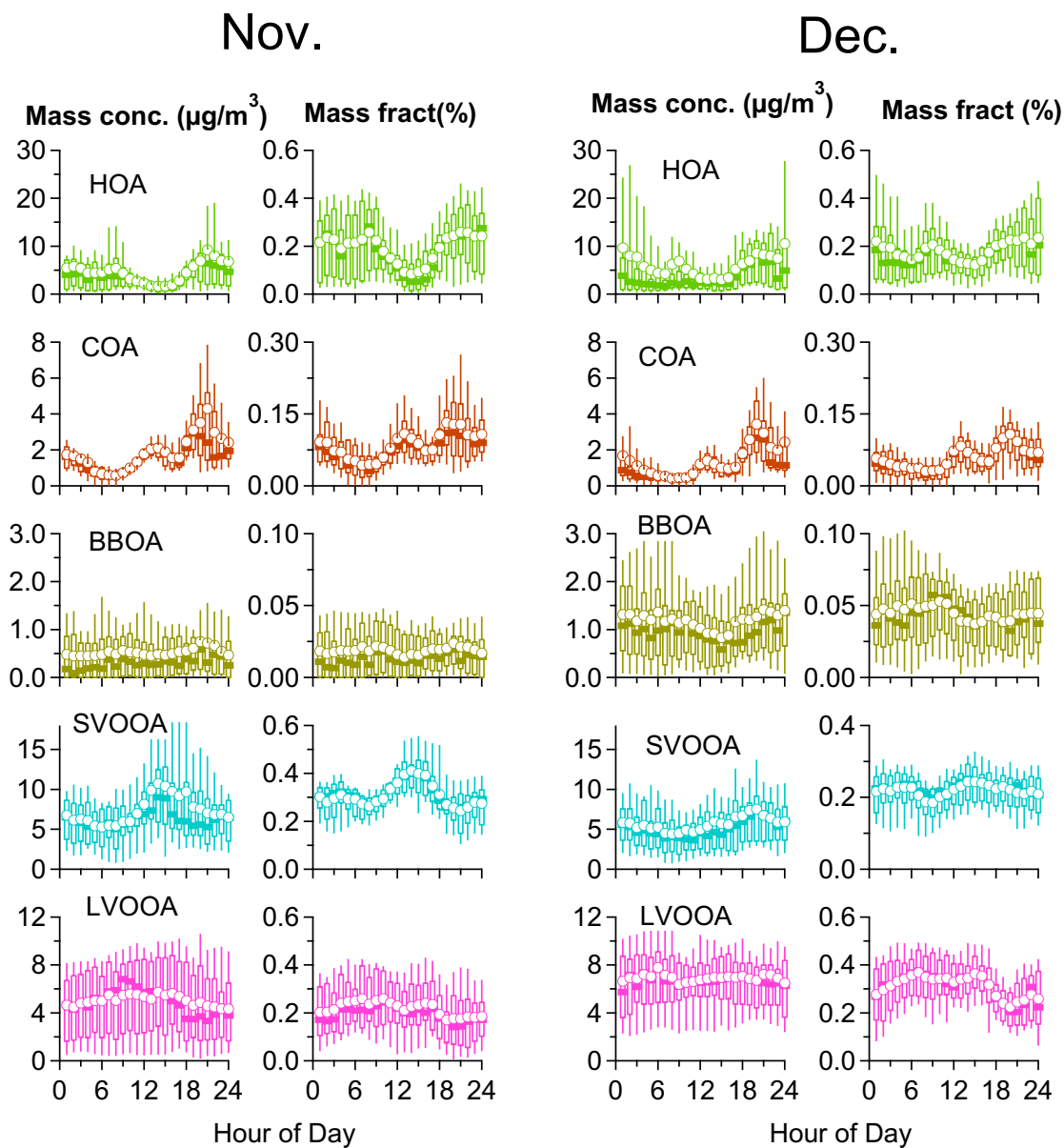
Figure 10. Diurnal variations in ME-2 resolved OA factors. Mass concentration of each OA factor (left). Mass fraction of each OA factor (right). 25th and 75th percentile boxes, 5th and 95th percentile whiskers, median as line in box, and mean as solid colored line.
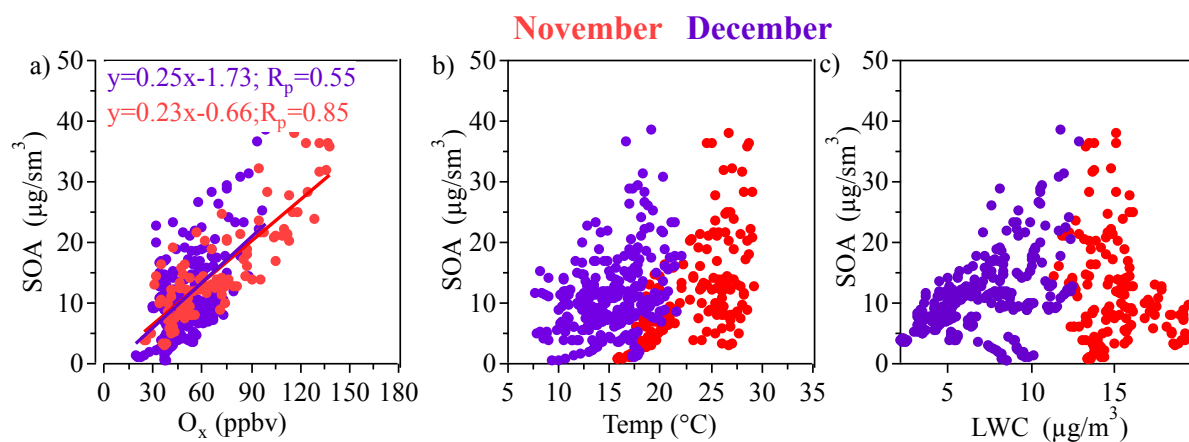
Figure 11. (a) SOA against Ox; (b)SOA against temperature; (c) SOA against LWC during the day. The concentration of SOA has been converted to standard temperature-pressure conditions to compare the slope of SOA/Ox with literature values.